Acta Crystallographica Section D
Biological Crystallography
ISSN 0907-4449

Structural analysis of a holoenzyme complex of mouse dihydrofolate reductase with NADPH and a ternary complex with the potent and selective inhibitor 2,4-diamino-6-(2′-hydroxydibenz[*b*,*f*]-azepin-5-yl)methylpteridine

Vivian Cody,[a,b]* Jim Pace[a] and Andre Rosowsky[c]

[a]Structural Biology Department, Hauptman–Woodward Medical Research Institute, 700 Ellicott Street, Buffalo, NY 14203, USA, [b]University of Buffalo, Buffalo, NY 14260, USA, and [c]Dana Farber Cancer Institute, Harvard Medical School, Boston, MA 02115, USA

Correspondence e-mail: cody@hwi.buffalo.edu

Received 27 May 2008
Accepted 16 July 2008

PDB References: dihydrofolate reductase complexes, 3d80, r3d80sf; 3d84, r3d84sf.

It has been shown that 2,4-diamino-6-arylmethylpteridines and 2,4-diamino-5-arylmethylpyrimidines containing an *O*-carboxylalkyloxy group in the aryl moiety are potent and selective inhibitors of the dihydrofolate reductase (DHFR) from opportunistic pathogens such as *Pneumocystis carinii*, the causative agent of *Pneumocystis* pneumonia in HIV/AIDS patients. In order to understand the structure–activity profile observed for a series of substituted dibenz[*b*,*f*]azepine antifolates, the crystal structures of mouse DHFR (mDHFR; a mammalian homologue) holo and ternary complexes with NADPH and the inhibitor 2,4-diamino-6-(2′-hydroxydibenz[*b*,*f*]azepin-5-yl)methylpteridine were determined to 1.9 and 1.4 Å resolution, respectively. Structural data for the ternary complex with the potent *O*-(3-carboxypropyl) inhibitor PT684 revealed no electron density for the *O*-carboxylalkyloxy side chain. The side chain was either cleaved or completely disordered. The electron density fitted the less potent hydroxyl compound PT684a. Additionally, cocrystallization of mDHFR with NADPH and the less potent 2′-(4-carboxybenzyl) inhibitor PT682 showed no electron density for the inhibitor and resulted in the first report of a holoenzyme complex despite several attempts at crystallization of a ternary complex. Modeling data of PT682 in the active site of mDHFR and *P. carinii* DHFR (pcDHFR) indicate that binding would require ligand-induced conformational changes to the enzyme for the inhibitor to fit into the active site or that the inhibitor side chain would have to adopt an alternative binding mode to that observed for other carboxyalkyloxy inhibitors. These data also show that the mDHFR complexes have a decreased active-site volume as reflected in the relative shift of helix *C* (residues 59–64) by 0.6 Å compared with pcDHFR ternary complexes. These data are consistent with the greater inhibitory potency against pcDHFR.

1. Introduction

Antifolates have been shown to be effective against dihydrofolate reductase (DHFR) from opportunistic pathogens such as *Toxoplasma gondii* (tg) and *Pneumocystis carinii* (pc), the causative agent of *Pneumocystis* pneumonia (PcP), which is still a cause of mortality among immunocompromised patients such as those with HIV/AIDS (Kovacs *et al.*, 2002; Thomas & Limper, 2004; Wakefield, 2002). The antifolate trimethoprim (TMP; Fig. 1), when used in combination with sulfamethox-

azole, synergistically targets the folate synthesis of these pathogens and is currently the preferred treatment for PcP (Stringer *et al.*, 2002; Cushion *et al.*, 2004). However, TMP has limited efficacy and drug resistance to TMP treatment is becoming more prevalent (Medrano *et al.*, 2005). These data illustrate the need for continued efforts to design more selective and potent inhibitors against these opportunistic infectious pathogens.

Recent structure activity data have shown that dibenz[*b*,*f*]azepines such as PT653 (Fig. 1) are moderately selective against pcDHFR and have a 100-fold increased binding preference for tgDHFR (Rosowsky *et al.*, 1999). These studies led to the structure-based design of a series of 2,4-diamino-6-[(ω-carboxyalkyl)oxy]dibenz[*b*,*f*]azepin-5-yl]pteridines that were more potent and selective than trimethoprim as inhibitors of DHFR from such opportunistic pathogens as *P. carinii*, *T. gondii* or *Mycobacterium avium* (Rosowsky *et al.*, 2004; Chan *et al.*, 2005). As illustrated in Table 1, these data revealed that the 2′-*O*-(3-carboxypropyl) analogue (PT684; Fig. 1) had the greatest inhibitory potency against pcDHFR, with an IC_{50} of 1.1 n*M* and a selectivity ratio of 1363 when compared with rat DHFR. Similarly, the 2′-*O*-(4-carboxybenzyl) analogue (PT682; Fig. 1) showed significant potency with an IC_{50} of 1.0 n*M* against pcDHFR, but had lower selectivity against the pathogenic DHFR and showed a selectivity ratio of 580 when compared with rat DHFR (Rosowsky *et al.*, 2004). These data suggest that modification of the 2′-position of the dibenz[*b*,*f*]-azepine ring contributes significantly to defining selectivity for the pathogenic DHFR enzymes. Computational models of the binding of the potent dibenz[*b*,*f*]azepine PT684 to human DHFR and pcDHFR has been carried out in order to better understand the selectivity profiles observed for this class of inhibitors (Rosowsky *et al.*, 2004). The crystal structures of the parent antifolate PT653 (Fig. 1) bound to pcDHFR (Cody *et al.*, 2002) and the tight-binding inhibitor PT523 (Fig. 1; Cody *et al.*, 1997) were used as starting models for these calculations. The results revealed a model in which the inhibitor carboxylate interacted with the conserved Arg in the active site, similar to that observed for other *O*-carboxyalkyloxy inhibitors (Cody *et al.*, 2006). These data suggested that differences in the interactions between the carboxylate of the inhibitor and Lys37 in pcDHFR and Gln35 in hDHFR could contribute to their enhanced selectivity for pcDHFR.

Table 1
Enzyme inhibition (IC_{50} in n*M*) against DHFR for selected inhibitors (Fig. 1; Chan *et al.*, 2005; Rosowsky *et al.*, 2004).

Inhibitor	pcDHFR	Rat DHFR	Rat DHFR/pcDHFR selectivity ratio
TMP	13000	180000	13.8
PTX	13	3.3	0.26
PT684	1.1	1500	1363
PT682	1.0	580	580
PT684a	31	14	1.3
PT653	79	3000	37.9

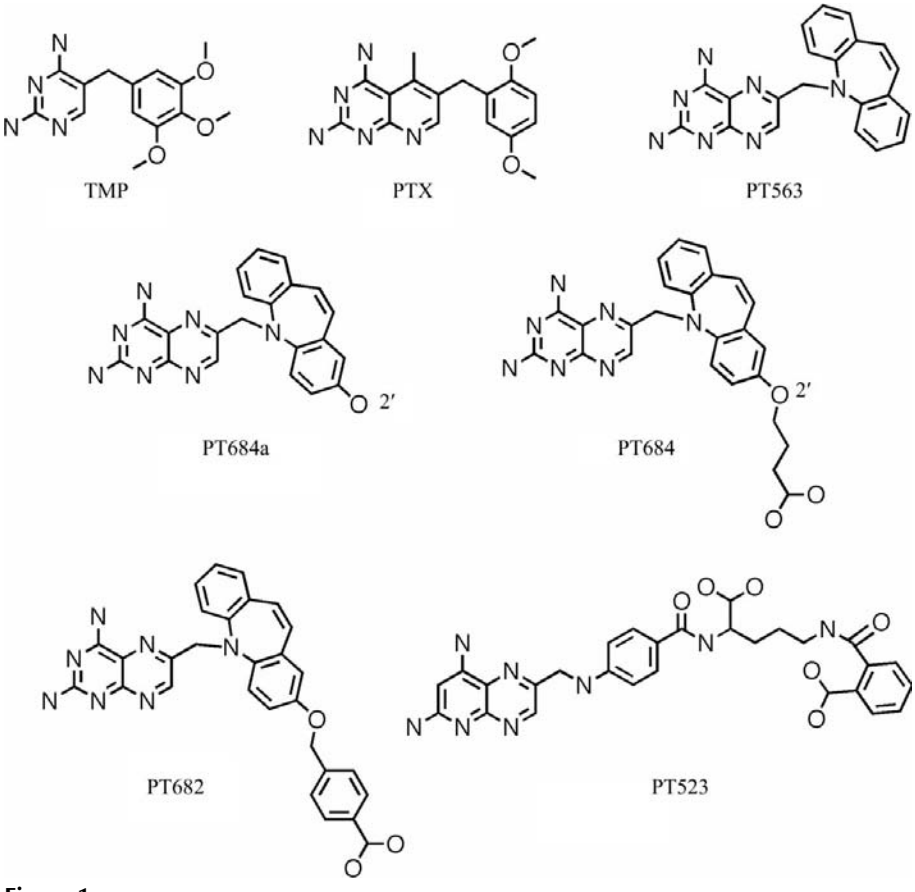

Figure 1
Schematic representations of the antifolates under study.

Based on the observations that the active-site residues of the mammalian DHFRs are highly conserved and that mouse DHFR (mDHFR) was easier to crystallize than human DHFR, we carried out structural studies using mouse DHFR. To better understand the mechanism of selectivity in binding to pcDHFR, the crystal structures of PT684 and PT682 were determined in complex with mouse DHFR and are compared with that of the parent benz[*b*,*f*]azepine PT653 (Fig. 1; Cody *et al.*, 2002). Efforts are also under way to crystallize these inhibitors with pcDHFR.

2. Methods

2.1. Expression of wild-type mDHFR

Recombinant mDHFR was expressed and purified as described previously (Pineda *et al.*, 2003). A single colony of *Escherichia coli* JM105 cells containing the pPH70D plasmid that harbors the fusion product of *E. coli* L54F DHFR and mDHFR linked with

Table 2
Data-collection and refinement statistics.

Values in parentheses are for the highest resolution shell.

	PT684a–NADPH	NADPH
Data collection		
Space group	$P2_1$	$P2_1$
Unit-cell parameters (Å, °)	a = 41.48, b = 61.30, c = 43.59, β = 117.22	a = 41.23, b = 61.17, c = 43.15, β = 118.26
Source	SSRL 9-1	R-AXIS IV
Resolution (Å)	1.00	1.90
Wavelength (Å)	1.00	1.5418
R_{merge}	0.083 (1.08)	0.034 (0.076)
R_{sym}† (%)	0.100 (1.49)	0.051 (0.48)
Completeness (%)	98.3 (97.4)	90.7 (50.5)
Observed reflections	38237	14951
Unique reflections	35455	13551
$I/\sigma(I)$	7.3 (0.7)	13.3 (2.5)
Multiplicity	3.4 (2.0)	15.1 (3.4)
Refinement and model quality		
Resolution range (Å)	31.61–1.40	23.83–1.90
No. of reflections	35455	12865
R factor‡	19.8	18.6
R_{free}§	21.3	21.0
Total protein atoms	1665	1665
Total ligand atoms	76	60
Total water atoms	319	82
Average B factor (Å^2)	19.7	19.0
R.m.s. deviation from ideal		
Bond lengths (Å)	0.011	0.018
Bond angles (°)	1.682	2.060
Ramachandran plot, residues in		
Most favored regions (%)	91.8	93.7
Additional allowed regions (%)	8.2	6.3
Generously allowed regions (%)	0.6	1.1
Disallowed regions (%)	0.0	0.0
PDB code	3d80	3d84

† $R_{sym} = \sum_{hkl}\sum_i |I_i(hkl) - \langle I(hkl)\rangle| / \sum_{hkl}\sum_i I_i(hkl)$, where $\langle I(hkl)\rangle$ is the mean intensity of a set of equivalent reflections. ‡ R factor = $\sum |F_{obs} - F_{calc}| / \sum F_{obs}$, where F_{obs} and F_{calc} are observed and calculated structure-factor amplitudes. § R_{free} was calculated as the R factor for a random 5% subset of all reflections.

thrombin was used to inoculate a 10 ml culture of Luria–Bertani (LB) broth (25 g l^{-1}) containing 50 µg ml^{-1} ampicillin. After incubation at 310 K overnight with shaking, one 10 ml culture was used to inoculate a 1 l culture of LB broth containing 50 µg ml^{-1} ampicillin. Bacteria were grown to an OD_{600} of 0.4–0.6, after which expression of mDHFR was induced by the addition of isopropyl β-D-1-thiogalactoside (IPTG) to a final concentration of 1 m*M*. After an induction time of 3 h, the cells were harvested by centrifugation at 277 K and 7000*g* for 30 min. The cell pellets were resuspended in 12.5 ml lysis buffer *A* (50 m*M* Tris, 5 m*M* EDTA, 50 µg ml^{-1} NaN_3, 10 ml protease-inhibitor cocktail pH 8.0) per gram of wet cells. The solution was left to incubate for 10 min at room temperature on a stir plate. 1.5 ml lysis buffer *B* (1.5 *M* sodium chloride, 0.1 *M* calcium chloride, 20 µg ml^{-1} DNase, 1 m*M* PMSF) per gram of wet cells was added. The solution was incubated for 10 min at room temperature on a stir plate. Dithiothreitol (DTT) was added to a final concentration of 5 m*M*. The sample was then subjected to six cycles of ultrasonic cell disruption for 15 s with intermittent cooling periods of 30 s on ice. The clarified supernatant was obtained by centrifugation at 277 K and 12 000 rev min^{-1} for 30 min.

2.2. Purification of mDHFR

The supernatant was dialyzed into PE buffer (20 m*M* potassium phosphate, 1 m*M* EDTA, 1 m*M* DTT pH 7.4). The protein was loaded at 0.5 ml min^{-1} onto a DEAE column equilibrated with PE buffer. The column was washed with 50 ml PE buffer with 1 m*M* DTT. The fusion protein, containing both *E. coli* DHFR L54F and mDHFR joined by a thrombin linker, was eluted with an 800 ml gradient of 0–0.5 *M*

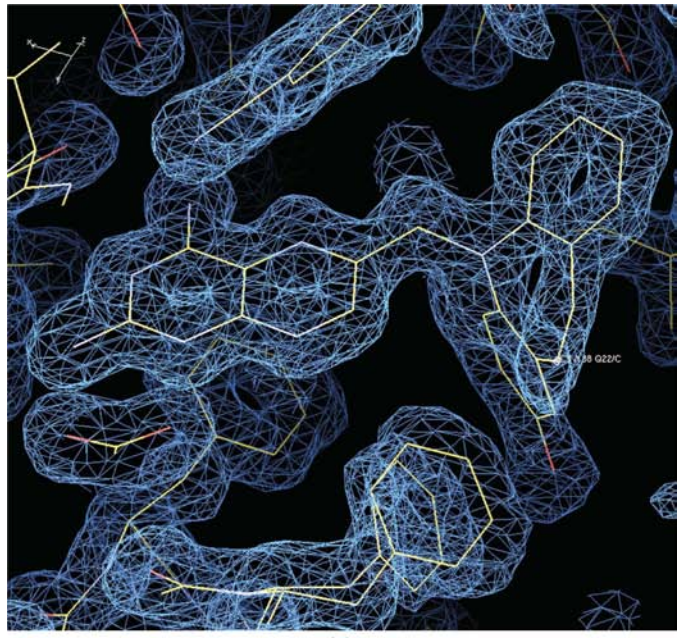

(*a*)

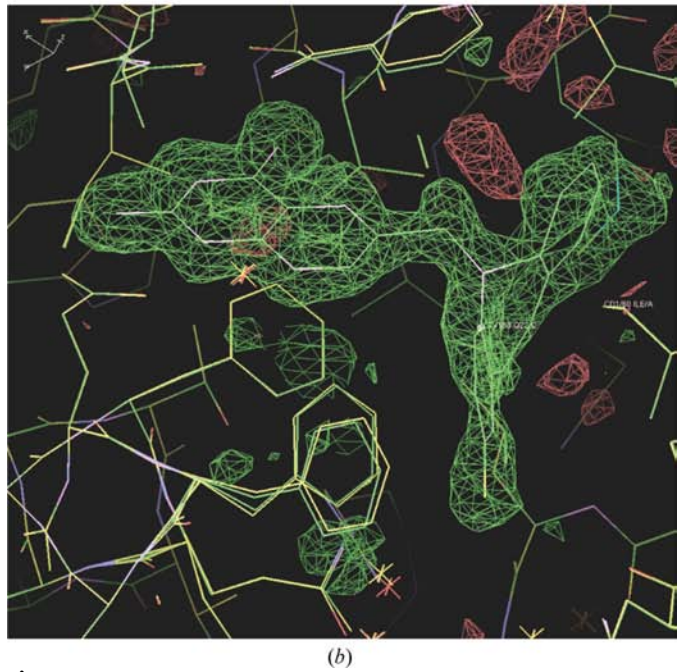

(*b*)

Figure 2
(*a*) Difference electron density ($2F_o - F_c$, 1.0σ) showing the inhibitor PT684a as a ternary complex with NADPH in mDHFR. Also shown are two alternate conformations for Phe31. (*b*) Difference electron density ($F_o - F_c$, 3σ) from an OMIT map calculated from the final refinement without inhibitor present. There is no indication of a partially occupied inhibitor side chain.

KCl. Fractions were monitored (Blakley, 1960) and those containing DHFR activity were pooled, concentrated using a YM-30 membrane and dialyzed into thrombin cleavage buffer (50 m*M* Tris, 0.1 *M* NaCl, 2.5 m*M* $CaCl_2$ pH 8.0). Cleavage of the fusion protein was initiated by the addition of 5 units of thrombin per milligram of fusion protein. The sample was left to incubate overnight (15–18 h) at 277 K. The next day, the protein was dialyzed for >3 h back into PE buffer containing freshly added DTT at 1 m*M* final concentration. The protein was then loaded onto a DEAE (GE Bioscience) column pre-equilibrated with PE buffer containing 1 m*M* DTT at 0.5 ml min^{-1}. After washing the column with 50 ml PE buffer containing 1 m*M* DTT, the cleaved mDHFR was eluted from the column using a 600 ml gradient of 0–0.1 *M* KCl. Fractions containing DHFR activity were pooled and concentrated using a YM10 membrane.

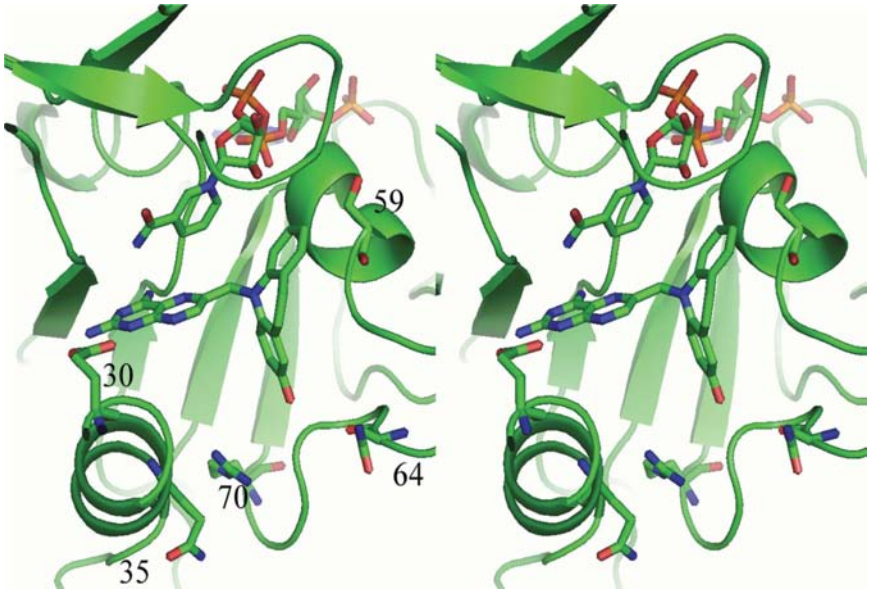

Figure 3
Stereoview of the ternary complex of NADPH and PT684a with mDHFR. The active-site residues Glu30, Gln35, Ser59, Asn64 and Arg70 are shown. This figure was drawn with *PyMOL*.

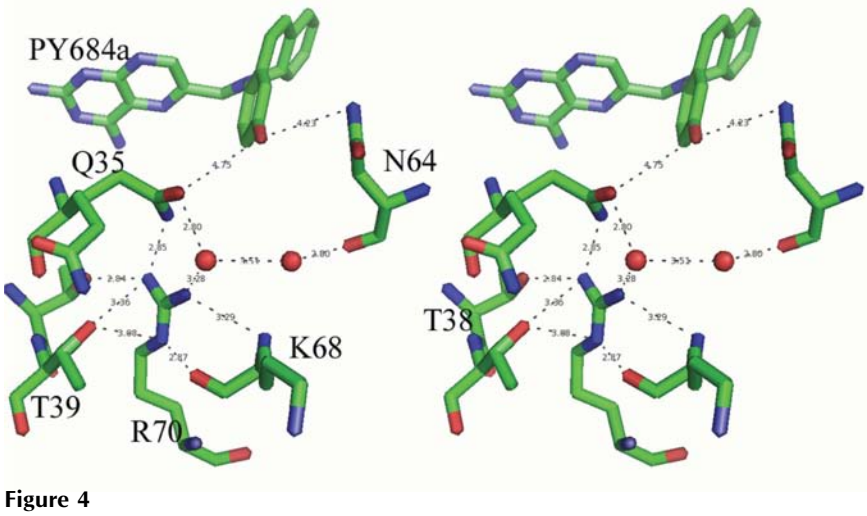

Figure 4
Stereoview of the conserved Arg70 interactions with their contact distances for the mDHFR–PT684a–NADPH ternary complex. This figure was drawn with *PyMOL*.

2.3. Crystallization

The protein was washed in a Centricon-10 with 10 m*M* HEPES buffer pH 7.4, concentrated to 27 mg ml^{-1} and incubated with NADPH and a 10:1 molar excess of the inhibitors 2,4-diamino-6-{2′-*O*-(3-carboxylpropyl)oxydibenz[*b*,*f*]azepin-5-yl}methylpteridine (PT684) or 2,4-diamino-6-{2′-*O*-(4-carboxybenzyl)oxydibenz[*b*,*f*]azepin-5-yl}methylpteridine (PT682) for 1 h over ice prior to crystallization using the hanging-drop vapor-diffusion method. Protein droplets contained 0.15 *M* Tris pH 8.3, 75 m*M* sodium cacodylate, 21% PEG 4K for the PT684 complex and 10 m*M* HEPES pH 7.4, 17 m*M* sodium acetate pH 6.5, 85 m*M* Tris–HCl and 25% PEG 4K for the PT682 complex. Crystals grew over several weeks and were treated with 15% glycerol as a cryoprotectant prior to mounting in the cold stream. The crystals of both complexes are monoclinic, space group $P2_1$, and diffracted to 1.4 and 1.9 Å resolution for PT684 and PT682, respectively. Data for the complex with PT684 were collected on beamline 9-1 at the Stanford Synchrotron Resource Laboratory (SSRL) using the remote-access protocol (McPhillips *et al.*, 2002; Cohen *et al.*, 2002; González *et al.*, 2008) and data for the PT682 complex were collected on a Rigaku R-AXIS IV imaging-plate system with MaxFlux optics. Data were processed using both *DENZO* (Otwinowski & Minor, 1997) and *MOSFLM* (Collaborative Computational Project, Number 4, 1994). Diffraction statistics are shown in Table 2 for both complexes.

2.4. Structure determination

The structures were solved by molecular-replacement methods using the coordinates of mDHFR (PDB code 2fzj; Cody *et al.*, 2006) in the program *MOLREP* (Collaborative Computational Project, Number 4, 1994). To monitor the refinement, a random subset of all reflections was set aside for the calculation of $R_{\rm free}$ (5%). Inspection of the resulting difference electron-density maps was made using the program *Coot* (Emsley & Cowtan, 2004) running on a Mac G5 workstation. The structures of the inhibitors were modeled based on those of PT653 (Fig. 1) reported in the structure of pcDHFR (Cody *et al.*, 2002) using the builder function in *SYBYL* (Tripos, St Louis, Missouri, USA) and the parameter files for

the inhibitors were prepared using the Dundee *PRODGR*2 server website (http://davapc1.bioch.dundee.ac.uk/programs/prodrg; Schüettelkopf & van Aalten, 2004). The final cycles of refinement were carried out using the program *REFMAC*5 from the *CCP*4 suite of programs (Collaborative Computational Project, Number 4, 1994). The Ramachandran conformational parameters from the last cycle of refinement generated by *PROCHECK* (Laskowski *et al.*, 1993) showed that more than 90% of the residues in both mDHFR complexes have the most favored conformation and that none are in disallowed regions. Coordinates for this structure have been deposited in the Protein Data Bank (PDB codes 3d80 and 3d84). Figures were prepared using the modeling program *PyMOL* (DeLano, 2006).

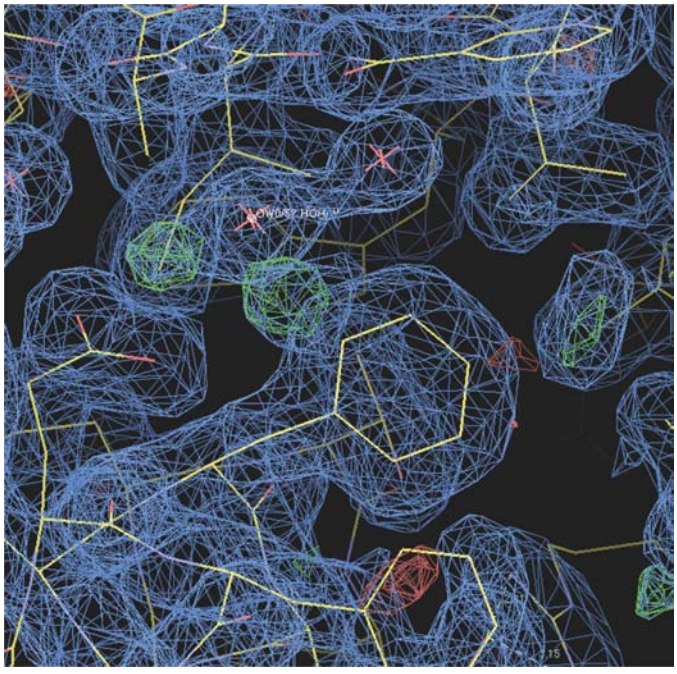

Figure 5
Difference electron density ($2F_o - F_c$, 1σ) for the holo complex with cofactor NADPH in mDHFR. The density in the active site was fitted to glycerol from the cryoprotection buffer.

3. Results

3.1. mDHFR ternary complex

Inspection of the difference electron-density map for the ternary complex of mDHFR with NADPH and what was initially assumed to be the carboxylic acid PT684 revealed no electron density for the 4-carboxypropyl side chain (Fig. 2). It is unclear whether the side chain is completely disordered in this region or whether the sample had decomposed on storage or on crystallization. One other possibility is that intramolecular catalysis had resulted in spontaneous cleavage of the carboxypropyl side chain during storage or under the crystallization conditions used, so that the molecule actually in the active site was the 2-hydroxydibenzazepine PT684a (Fig. 3). The side chains of Phe31 and Gln35 were also observed in two alternate conformations in this complex. There is a partial water molecule present in one of the Gln35 conformers that also contacts Arg70 when the partially occupied Gln35 is not present.

The more surprising observation for these data is the lack of involvement of the putative hydroxyl group of PT684a in any hydrophilic interactions. The closest contact of the hydroxyl group of PT684a is with a partially occupied conformer of Phe31 (2.9 Å), while the other contact distances range from 3.7 to 4.7 Å to the partially occupied water/Gln35 and the side chains of Asn64 and Leu60 (Fig. 4).

As previously described in the structures of mDHFR–inhibitor complexes (Cody *et al.*, 2005, 2006; Cody & Schwalbe, 2006), the orientation of the conserved Arg70 is held in place by a network of hydrogen bonds with the conserved Thr38 and Thr39 and the backbone functional groups of Lys68 and through water to the backbone carbonyl of Asn64. There are also contacts to other structural water molecules in the active pocket (Fig. 4).

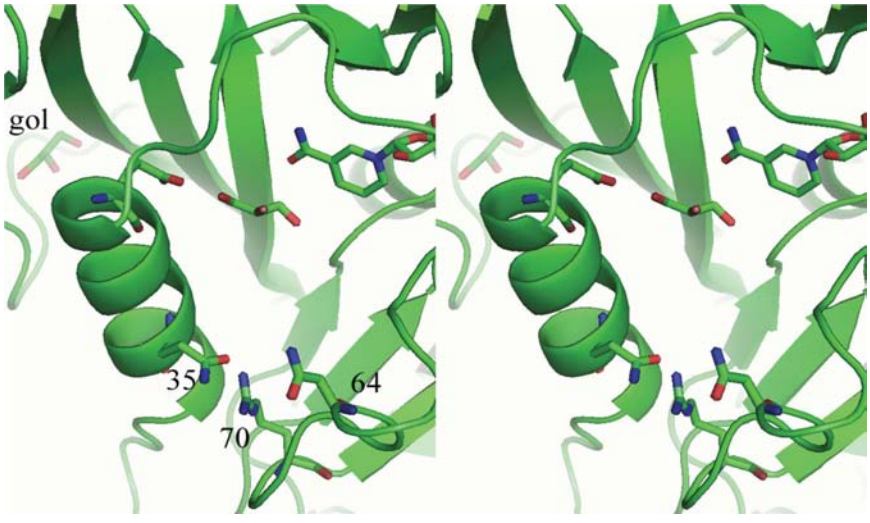

Figure 6
Stereoview of mDHFR with NADPH and a glycerol molecule in the active site of the holo structure. Residues Glu30, Gln35, Asn64 and Arg70 are shown. This figure was drawn with *PyMOL*.

3.2. mDHFR holoenzyme complex

When the difference density maps were analyzed for the complex with PT682, it was shown that the final structure is a holoenzyme complex containing only the cofactor NADPH (Fig. 5). Although diffraction data from three separate crystallization trials were collected, all crystals were found to be holoenzyme complexes. This is the first report of a mammalian DHFR holo complex structure. The active site is occupied by a molecule of glycerol

used as a cryoprotection agent during diffraction data collection (Fig. 6).

3.3. Overall structure

There are no significant changes in the overall structure of the holo and ternary mDHFR complexes (r.m.s.d. = 0.38 Å between all residues in these two structures), which also are similar to previously reported mDHFR structures (Cody *et al.*, 2005, 2006). The interactions of the 2,4-diaminopteridine ring of PT684a preserves the overall pattern of contacts with invariant residues in the active site as observed in other DHFR–inhibitor complexes (Cody & Schwalbe, 2006). The intermolecular interactions of PT684a are also similar to those observed for the parent compound PT653 reported in the crystal structure with pcDHFR (Cody *et al.*, 2002; Fig. 7); the 4-amino group makes a number of hydrogen-bond contacts with the backbone functional groups of Ile7 (2.9 Å) and Val115 (3.1 Å) and the side chains of Tyr121 (3.4 Å) and the nicotinamide of NADPH (3.5 Å) that contribute to the tight binding of antifolates. There is an invariant hydrogen-bond network involving structural water, the conserved residues Thr136, Glu30 and Trp24 and the N1 nitrogen and 2-amino group of PT684a. The pteridine ring N8 makes contacts to Glu30 and Trp24 through a structural water molecule that is observed in most DHFR structures.

Comparison of these mDHFR complexes with those of the parent PT653 bound to pcDHFR (Cody *et al.*, 2002) and with methotrexate (MTX) bound to mouse and human DHFR (Cody *et al.*, 2006) reveals that the backbone of helix *C* (encompassing residues 59–64; human numbering) is displaced by 0.2–1.3 Å depending on the ligand bound and reflects ligand-induced conformational changes (Cody *et al.*, 1999). Measurements of the distances between the C^{α} atom of residue Glu30 and the C^{α} atoms of residues Asp21, Leu22, Ser59 and Leu60 (Table 3) describe the relative size of the active site in these structures. As illustrated, the largest differences measured at positions 59 and 60 are between the human DHFR–MTX complex (Cody *et al.*, 2005) and the pcDHFR–PT653 complex (Cody *et al.*, 2002) with a shift of 1.3 Å in the relative position of helix *C*, making the pcDHFR active site larger as a result of ligand-induced conformational changes (Cody *et al.*, 1999; Fig. 8). The difference between the helix *C* positions of mDHFR–PT684a and hDHFR–MTX is 0.7–1.3 Å. It is somewhat surprising to note that there is little change in these contact distances between the holo and PT684a ternary complex with mDHFR (Table 3). These data suggest that the MTX ternary complexes are more tightly bound and that the human enzyme has the smallest active-site volume.

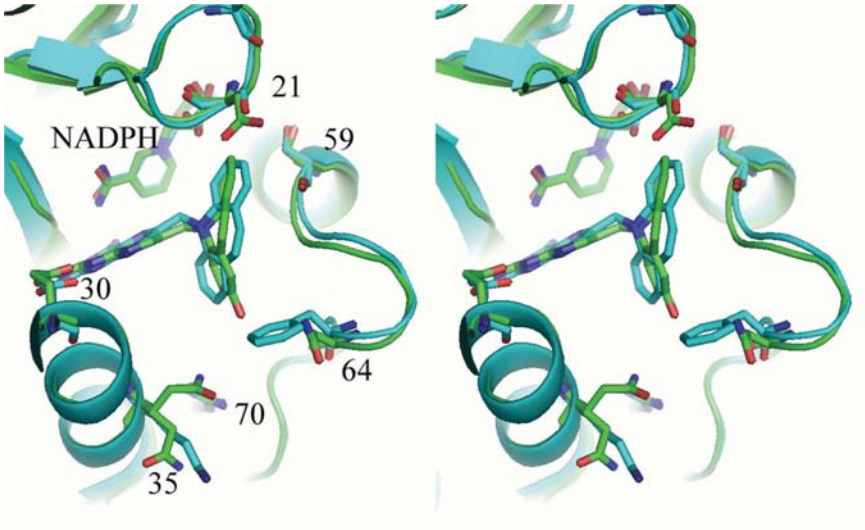

Figure 7
Stereo superposition of the mDHFR ternary complex with PT684a (green) and the pcDHFR (cyan) ternary complex with NADPH and inhibitor PT653 (Cody *et al.*, 2002). The mDHFR sequence numbers are shown for the active-site residues. This figure was drawn with *PyMOL*.

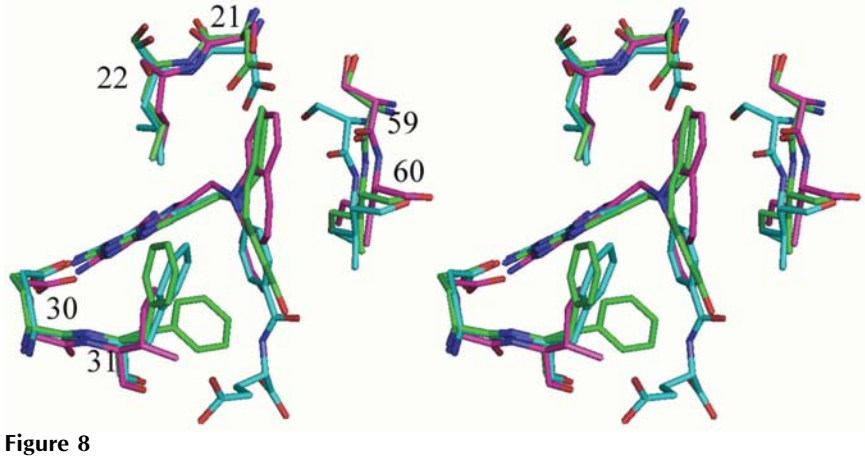

Figure 8
Stereo comparison of mDHFR–NADPH–PY684a (green), hDHFR–MTX–NADPH (Cody *et al.*, 2005; cyan) and pcDHFR–NADPH–PT653 (Cody *et al.*, 2002; violet), highlighting the conformation of loop 21 and helix *C* with residues Ser59 and Leu60 in all structures. Residues are numbered for the mammalian enzyme. Position 21 is Asp in the mammalian DHFR and Ser in pcDHFR, 22 is Leu in all structures, 30 is Glu in all three structures and 31 is Phe in mammalian and Ile in pcDHFR. This figure was drawn with *PyMOL*.

4. Discussion

These structural studies describe the binding of a hydrolyzed product PT684a (Fig. 1) as a ternary complex with NADPH and mDHFR; no electron density was evident for the carboxyalkyloxy side chain. There was also no evidence of a partially occupied position for the side chain. These observations suggest that the side chain is completely disordered or has been cleaved under the storage or crystallization conditions

Table 3
Contact distances (Å) between active-site residues in DHFR complexes.

	Residue C^{α}			
	30···22	30···21	30···59	30···60
mDHFR–PT684a	12.2	15.1	17.5	15.3
Holo mDHFR	12.3	15.3	17.2	15.3
mDHFR L22R–MTX†	12.1	14.5	16.5	14.8
hDHFR–MTX†	12.2	14.7	16.2	14.6
pcDHFR–PT653‡	12.3	15.1	17.9	15.9
pcDHFR–MTX§	11.7	15.0	16.5	14.7

† Cody *et al.* (2005). ‡ Cody *et al.* (2002). § Cody *et al.* (1999).

used, resulting in density that is consistent with the hydroxyl compound PT864a. This product was shown to be less potent (Table 1) than those that contain a carboxylate side chain that can interact with the conserved Arg70 present in all DHFRs. Comparison of this complex with the parent dibenz[*b*,*f*]aze-]azepine PT653 (Cody *et al.*, 2002; Fig. 7) reveals only small variations in the buckling of the dibenz[*b*,*f*]azepine ring compared with the mDHFR complex.

One of the strategies developed for the design of these dibenz[*b*,*f*]azepine antifolates was to probe the binding interactions in the flexible loop near residues 20–24 of the DHFR active site. Thus, by making a rigid group that could occupy this region while still occupying the *p*-aminobenzoyl glutamate portion of the substrate active-site pocket, it would be possible for this rigid group to exploit differences in the active-site volume that result from movement of the flexible loop 20–24 between the mammalian and fungal DHFR enzymes (Rosowsky *et al.*, 1999). Comparison of the loop 20–24 positions in the structures of the human, mouse and *P. carinii* DHFR complexes with MTX and the dibenz[*b*,*f*]-azepine antifolates reveals that the greatest difference is between the hDHFR–MTX complex and the mDHFR complex with PT684a, as measured by the differences in the distance from the C^{α} atom of Glu30 to those of Asp21 and Leu22 (Table 3, Fig. 8). These data reveal a progressive increase in the distance for the pcDHFR–MTX, pcDHFR–PT653 and mDHFR–PT684a ternary complexes, respectively. It is somewhat surprising that the mDHFR holoenzyme complex has the same contact distances as the PT684a ternary complex.

Similarly, the effects of ligand-induced conformational changes are reflected in the relative movement of helix *C* (residues 59–64), which indicates an increase in the active-site size among these species. However, in this case the largest shift is observed for the PT653 ternary complex with pcDHFR, which has a 1.3 Å displacement at residue Leu60 of helix *C* relative to the human DHFR–MTX ternary complex (Table 3). The change for the mDHFR ternary complex with PT684a is 0.7 Å relative to the 0.4 Å difference for the pcDHFR–MTX complex.

These data also show that the complex with the highly selective inhibitor PT682 resulted in the first report of a mammalian holo mDHFR enzyme complex with the cofactor NADPH. Despite efforts to cocrystallize PT682 as a ternary complex with mDHFR, only the holoenzyme complex was observed. Modeling studies of the binding of PT682 to mDHFR and pcDHFR indicate that an alternate binding mode is needed for this inhibitor to fit into the active site. If in both mDHFR and pcDHF the binding of PT682 is similar to that observed for PT653 in pcDHFR (Cody *et al.*, 2002), then the carboxylate side chain has steric clashes with the conserved Arg in the active site (Fig. 9). The fact that PT684 has significant potency and selectivity in pcDHFR would suggest that ligand-induced conformational changes need to occur for inhibitor binding or that the carboxyalkyloxy side chain can adopt an alterative conformation and forgo interaction with Arg, as observed in other carboxyalkyloxy inhibitors (Cody *et al.*, 2006). These data may indicate that the steric bulk of this antifolate is such that it is prevented from binding to any significant degree in mDHFR. These models for the binding of PT682 are in contrast to those derived for the binding of PT684, in which the carboxylate was shown to interact with the conserved Arg in both pcDHFR and hDHFR (Rosowsky *et al.*, 2004). These data are the first to illustrate the lack of binding to mammalian DHFR to explain its loss of potency compared with pcDHFR.

Crystallization screens are under way to obtain complexes of pcDHFR with the potent dibenz[*b*,*f*]azepine antifolates PT684 and PT682 in order to validate the computational models that suggested that interactions of the 2′-(ω-carboxyalkyloxy) or 2′-(4-carboxybenzyloxy) substitutent with the conserved active-site Arg70 and the differential interactions with Gln35 in mammalian *versus* Lys37 in pcDHFR contribute to their high potency and selectivity against the pathogenic DHFR enzymes.

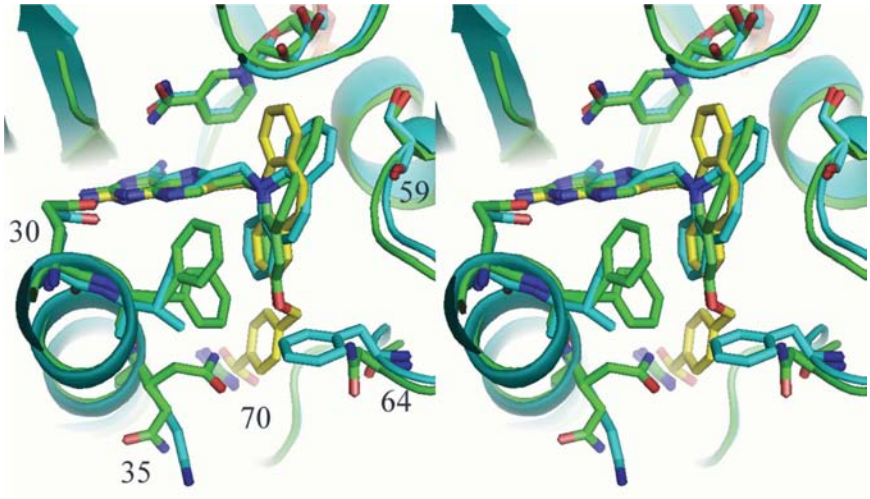

Figure 9
Stereo comparison of the ternary complex of mDHFR with NADPH and PT684a (green), pcDHFR with PT653 (cyan; Cody *et al.*, 2002) and a model of PT682 (yellow). Note that the carboxylate group clashes with Arg70.

This work was supported in part by grants from the National Institutes of Health GM51670 (VC). The authors thank the beamline 9-1 staff at SSRL for their support. Portions of this research were carried out at the Stanford Synchrotron Radiation Laboratory, a national user facility operated by Stanford University on behalf of the US Department of Energy, Office of Basic Energy Sciences. The SSRL Structural Molecular Biology Program is supported by the Department of Energy, Office of Biological and Environmental Research and by the National Institutes of Health, National Center for Research Resources, Biomedical Technology Program and the National Institute of General Medical Sciences.

References

Blakley, R. L. (1960). *Nature (London)*, **188**, 231–232.
Chan, D. C. M., Fu, H., Forsch, R. A., Queener, S. F. & Rosowsky, A. (2005). *J. Med. Chem.* **48**, 4420–4431.
Cody, V., Galitsky, N., Luft, J. R., Pangborn, W., Rosowsky, A. & Blakley, R. L. (1997). *Biochemistry*, **36**, 13897–13903.
Cody, V., Galitsky, N., Luft, J. R., Pangborn, W., Rosowsky, A. & Queener, S. F. (2002). *Acta Cryst.* D**58**, 946–954.
Cody, V., Galitsky, N., Rak, D., Luft, J. R., Pangborn, W. & Queener, S. F. (1999). *Biochemistry*, **38**, 4303–4312.
Cody, V., Luft, J. R. & Pangborn, W. (2005). *Acta Cryst.* D**61**, 147–155.
Cody, V., Pace, J., Chisum, K. & Rosowsky, A. (2006). *Proteins*, **65**, 959–969.
Cody, V. & Schwalbe, C. H. (2006). *Crystallogr. Rev.* **12**, 301–333.
Cohen, A. E., Ellis, P. J., Miller, M. D., Deacon, A. M. & Phizackerley, R. P. (2002). *J. Appl. Cryst.* **35**, 720–726.
Collaborative Computational Project, Number 4 (1994). *Acta Cryst.* D**50**, 760–763.
Cushion, M. T., Keely, S. P. & Stringer, J. R. (2004). *Mycologia*, **96**, 429–438.
DeLano, W. L. (2006). *MacPyMOL.* http://www.pymol.org.
Emsley, P. & Cowtan, K. (2004). *Acta Cryst.* D**60**, 2126–2132.
González, A., Moorhead, P., McPhillips, S. E., Song, J., Sharp, K., Taylor, J. R., Adams, P. D., Sauter, N. K. & Soltis, S. M. (2008). *J. Appl. Cryst.* **41**, 176–184.
Kovacs, J. A., Gill, V. J., Meshnick, S. & Maur, H. (2002). *J. Am. Med. Assoc.* **286**, 2450–2460.
Laskowski, R. A., MacArthur, M. W., Moss, D. S. & Thornton, J. M. (1993). *J. Appl. Cryst.* **26**, 283–291.
McPhillips, T. M., McPhillips, S. E., Chiu, H.-J., Cohen, A. E., Deacon, A. M., Ellis, P. J., Garman, E., Gonzalez, A., Sauter, N. K., Phizackerley, R. P., Soltis, S. M. & Kuhn, P. (2002). *J. Synchrotron Rad.* **9**, 401–406.
Medrano, F. J., Montes-Cano, M., Conde, M., de la Horra, C., Respaldiza, N., Gasch, A., Peres-Lozano, M. J., Varela, J. M. & Calderon, E. J. (2005). *Emerg. Infect. Dis.* **11**, 245–250.
Otwinowski, Z. & Minor, W. (1997). *Methods Enzymol.* **276**, 307–326.
Pineda, P., Kanter, A., McIvor, R. S., Benkovic, S. J., Rosowsky, A. & Wagner, C. R. (2003). *J. Med. Chem.* **46**, 2816–2818.
Rosowsky, A., Cody, V., Galitsky, N., Fu, H., Papoulis, A. T. & Queener, S. F. (1999). *J. Med. Chem.* **42**, 4853–4860.
Rosowsky, A., Fu, H., Chan, D. C. M. & Queener, S. F. (2004). *J. Med. Chem.* **47**, 2475–2485.
Schüttelkopf, A. W. & van Aalten, D. M. F. (2004). *Acta Cryst.* D**60**, 1355–1363.
Stringer, J. R., Beard, C. B., Miller, R. F. & Wakefield, A. E. (2002). *Emerg. Infect. Dis.* **8**, 891–896.
Thomas, C. F. & Limper, A. H. (2004). *N. Engl. J. Med.* **350**, 2487–2498.
Wakefield, A. (2002). *Brit. Med. Bull.* **61**, 175–188.